Development of $MgAl_2O_4$ grain refiner in Al in-situ composite through H_3BO_3 addition

Development of $MgAl_2O_4$ grain refiner in Al in-situ composite through H_3BO_3 addition

***P Chandramohan[1,2], P A Olubambi[2], R Raghu [1]and B A Obadele[2]**

[1]Department of Mechanical Engineering, Sri Ramakrishna Engineering College, Coimbatore 641 022, India

[2]School of Mining, Metallurgy and Chemical Engineering, University of Johannesburg, South Africa 2028

*E-mail: pcmohu@yahoo.co.in

Abstract. In the present work, a novel approach has been made for synthesis of in-situ Magnesium Aluminate ($MgAl_2O_4$) particles in the Al-4Mg alloy by Boric Acid (H_3BO_3) precursor addition (1 wt %, 1.5 wt % and 2 wt %) during the casting process. The developed composite has been investigated for its microstructural characteristics and corrosion performance. Scanning Electron Microscopy and Energy Dispersive Spectroscopy examination revealed the formation of $MgAl_2O_4$ particles in the composite. Potentiodynamic polarization corrosion experiments were performed on the Al-4Mg/H_3BO_3 composite specimens (1 wt %, 1.5 wt % and 2 wt %) in three different medium (3.5 % Sodium Chloride-NaCl, 1 M Sulphuric Acid-H_2SO_4 and 1 M Hydrochloric Acid-HCl). Corrosion results showed that Al-4Mg/1.5 wt % H_3BO_3 composite specimen exhibited better corrosion resistance in 3.5 % NaCl, 1 M H_2SO_4 and 1 M HCl medium due to the significant grain refinement produced by $MgAl_2O_4$ particles. The developed composite with better corrosion properties can be utilized for marine and naval application.

1. Introduction

Aluminium 5xxx series alloys (Al-Mg) are widely used in the transportation field, marine industry and other industries due to their better corrosion resistance and weldability [1,2]. Among 5xxx series alloys, the 5083 alloy (Al-4Mg) contains Mg as the solute alloying element, which aids in improvement of corrosion performance. However, the 5083 alloy containing more than 3 % Mg suffers from intergranular and pitting corrosion because of β phase (Al_3Mg_2) precipitation at the grain boundaries [3,4]. Corrosion attack in this alloy reduces the lifetime of the component and safety of the application [5, 6]. It is therefore highly essential to control the corrosion resistance in these aluminium alloys.

The corrosion behaviour of aluminium relies on several factors such as the condition of the material, microstructural features of the material and the electrolyte. Among these, microstructure affects the corrosion of the alloy significantly [7-9]. Various researchers have attempted to increase the corrosion resistance of aluminium alloys through the addition of elements such as Strontium (Sr), Neodymium (Nd) and Zinc (Zn) [10-12]. It is stated that grain refinement in the aluminium alloy improves the corrosion resistance [13]. Traditionally, addition of inoculants is the commonly approach for grain refinement and also distribution of the second phase in the aluminium alloy [14-17]. Various methods

have been attempted by several researchers to produce grain refinement in the 5083 aluminium alloy for better corrosion performance.

Ali Torkan et al. (2018) [18] investigated the microstructural and corrosion characteristics of the accumulative roll bonded (2, 4 and 6 passes) aluminium alloy (5083) in 3.5% NaCl solution. Microstructural examination of the aluminium alloy revealed that accumulative roll bonding aids in development of nanostructured (up to 10 nm) microstructure. Polarization tests were carried out on the aluminium specimens and it was reported that the corrosion rate decreases up to 4 passes and then increases. Shuiqing Liu et al. (2019) [19] attempted to improve the corrosion performance of 5083 aluminium alloy through the addition of nano-Cerium Hexaboride (CeB_6)/Al inoculant. Potentiodynamic polarization tests were carried out on the inoculated alloy, in a 3.5 wt% NaCl solution, and its corrosion performance was compared to a cold-rolled alloy and as-cast alloy. It was observed that grain refinement (up to 100 μm) occurred with the addition of nano-CeB_6/Al inoculant, which resulted in high corrosion resistance better than the other two alloys.

Sadegh Rasouli et al. (2014) [20] used a Friction Stir Processing (FSP) technique to improve the microstructural and mechanical properties of the AA5083 aluminum alloy. It is observed that dynamic recrystallization resulted due to intense plastic deformation produced during FSP. Polarization tests performed on the FSPed alloy resulted in higher corrosion resistance than base metal which is due to the microstructural refinement caused by FSP.

Various techniques are available for grain refinement of the Al5083 alloy. Among those, recently developed technique is the generation of the Al5083 composites through the addition of reinforcements. Prabhakar et al. (2018) [21] fabricated the Al5083 aluminum/fly ash surface composites through friction stir processing (FSP) under different speeds and feed rates, and investigated its mechanical properties. Results revealed that the FSPed composite (97.2 HV) has higher hardness than the FSPed alloy (83.5 HV) and unprocessed alloy (68.3 HV) which is attributed to the grain refinement due to the addition of flyash.

Meijuan Li et al. (2016) [22] developed a nanostructured Al5083/nano-Titanium Diboride (TiB_2) composite through cryomilling and spark plasma sintering (SPS). Microstructural observation revealed greater refinement of the Al matrix having an average grain size of ~74 nm and a homogeneous distribution of (n-TiB_2) in the Al matrix. Ranjit Bauri et al. (2014) [23] incorporated tungsten particles in the aluminium 5083 matrix through FSP and studied its microstructural and mechanical properties. Uniform dispersion and greater interfacial bonding was observed between the tungsten and aluminium matrix. Results revealed that Ultimate Tensile Strength (UTS) of the composite increased more than 100 MPa and ductility increased up to 30 % which is due to substantial grain refinement of the matrix because of dynamic recrystallization.

From the literature review, it is observed that various research has concentrated on the microstructural and mechanical properties of Al5083 alloy and ex-situ 5083 composites. It is observed that in these studies, the improvement of properties was attained through grain refinement. However, the development of in-situ Al composite has rarely been reported. In addition, corrosion behaviour of such composites has not been investigated. Hence in the present study, Al5083 (Al-4Mg) alloy was prepared in the laboratory and in-situ Al-4Mg/$MgAl_2O_4$ composite was produced with the addition of H_3BO_3 (1 wt %, 1.5 wt % and 2 wt %). It is anticipated that the addition of $MgAl_2O_4$ in the alloy will aid in grain refinement and improvement of corrosion resistance.

2. Experimental procedure

Al-4Mg alloy was cast using Electrical Conductor (EC) grade pure aluminium and commercial grade pure magnesium, melted using an electric resistance furnace. H_3BO_3 of varying wt.% (1, 1.5 and 2) with an average grain size of 20 μm was taken as the oxide source and incorporated into the Al-4Mg melt. H_3BO_3 is an oxide source which tends to react with the Al and forms $MgAl_2O_4$ reinforcement. The melt is kept at 750 °C for 15 min to aid the reaction of Al-4Mg melt with H_3BO_3. The melt is then poured into the die. The final product is a composite that was examined through Scanning Electron Microscope (SEM) with Energy Dispersive Spectrometer (EDS), to observe the morphology and confirm the presence of $MgAl_2O_4$.

Al-4Mg/$MgAl_2O_4$ in-situ composite specimens were taken for potentiodynamic polarization experiments and the experiments were conducted (Potentiostat - Autolab 302 NFRA2, Metrohm). The electrochem system is equipped with Nova 2.1 software which is used for Tafel extrapolation. For the corrosion experiments, a platinum rod is taken as the counter electrode, saturated silver/silver chloride (Ag/AgCl) as the reference electrode and the Al-4Mg/ H_3BO_3 composite specimens were taken as the working electrode. Polarization experiments were conducted from -0.3 V to 2 V at a scan rate of 2 mV s^{-1} using three different solutions 3.5 % NaCl, 1 M H_2SO_4 and 1 M HCl at room temperature.

3. Results and discussion

The $MgAl_2O_4$ products are produced due to various reactions through the reactive wetting of the H_3BO_3 and the Al-4Mg melt [24-26]

$4H_3BO_{3(s)} \rightarrow 2B_2O_{3(s)} + 6H_2O_{(g)}$, $T = 200°C$ (1)

$B_2O_{3(s)} \rightarrow B_2O_{3(l)}$, $T = 450°C$ (2)

$B_2O_{3(l)} + 3\,Mg \rightarrow 3MgO + 2B$, $T = 650°C$ (3)

$B_2O_{3(l)} + 2Al + MgO \rightarrow MgAl_2O_4 + 2B$, $T = 650°C$ (4)

Reaction products formed tend to increase the wettability between the reinforcement and the melt. The interfacial energy is reduced due to the reaction between the substrate and the reinforcement. The displacement reactions (3) and (4) take place consequently and the reaction products such as MgO or $MgAl_2O_4$ are formed at molten metal/particle interfaces. The presence of Al and Mg at the reaction zone aids the MgO and $MgAl_2O_4$ formation. It is anticipated that MgO formation takes place easier than $MgAl_2O_4$ due to greater reactivity of Mg than Al. MgO transforms into $MgAl_2O_4$ particles upon diffusion of Al atom.

3.1. SEM and EDS analysis

SEM examination has been carried out in the Al-4Mg/1, 1.5 and 2 wt% H_3BO_3 composite specimens to observe the morphology of the $MgAl_2O_4$. EDS was done to confirm the formation of $MgAl_2O_4$ crystals. The polygonal faceted type $MgAl_2O_4$ crystals are observed in the microstructures of the Al-4Mg/1, 1.5 and 2 wt% H_3BO_3 composite specimens and successfully distributed in the Al-Mg matrix through the addition of H_3BO_3 as shown in Figure 1a-c. This was also confirmed by the EDS spectra that show the presence of Mg, Al and O in the $MgAl_2O_4$ crystals (Figure 2a-c).

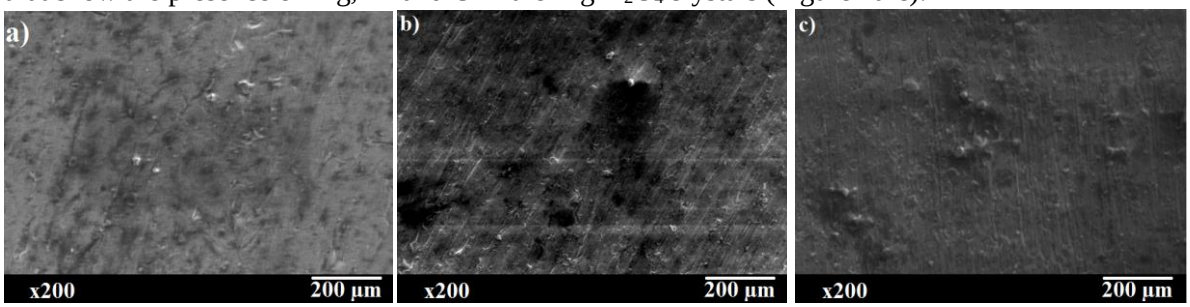

Figure 1.SEM micrograph of the Al-4Mg/H_3BO_3 composite specimen at lower magnification (a) 1 wt % (b) 1.5 wt % and (c) 2 wt %.

Nevertheless, the size and quantity of the $MgAl_2O_4$ crystals formed in the composite specimens are different. The average size and fraction of the reinforcement particles has been determined through the Image analysis software Image J. In the Al-4Mg-1 wt % H_3BO_3, the size of the $MgAl_2O_4$ crystals found very small (4 µm) and number of particles formed is also less (1.5 %). In the Al-4Mg-1.5 wt % H_3BO_3, an increased amount (2.3 %) of $MgAl_2O_4$ with a medium size (6.36 µm) is formed and upon further increase in H_3BO_3 (2 wt %), the amount (3.3 %) and size (7.5 µm) of $MgAl_2O_4$ crystals increases with few agglomerations.

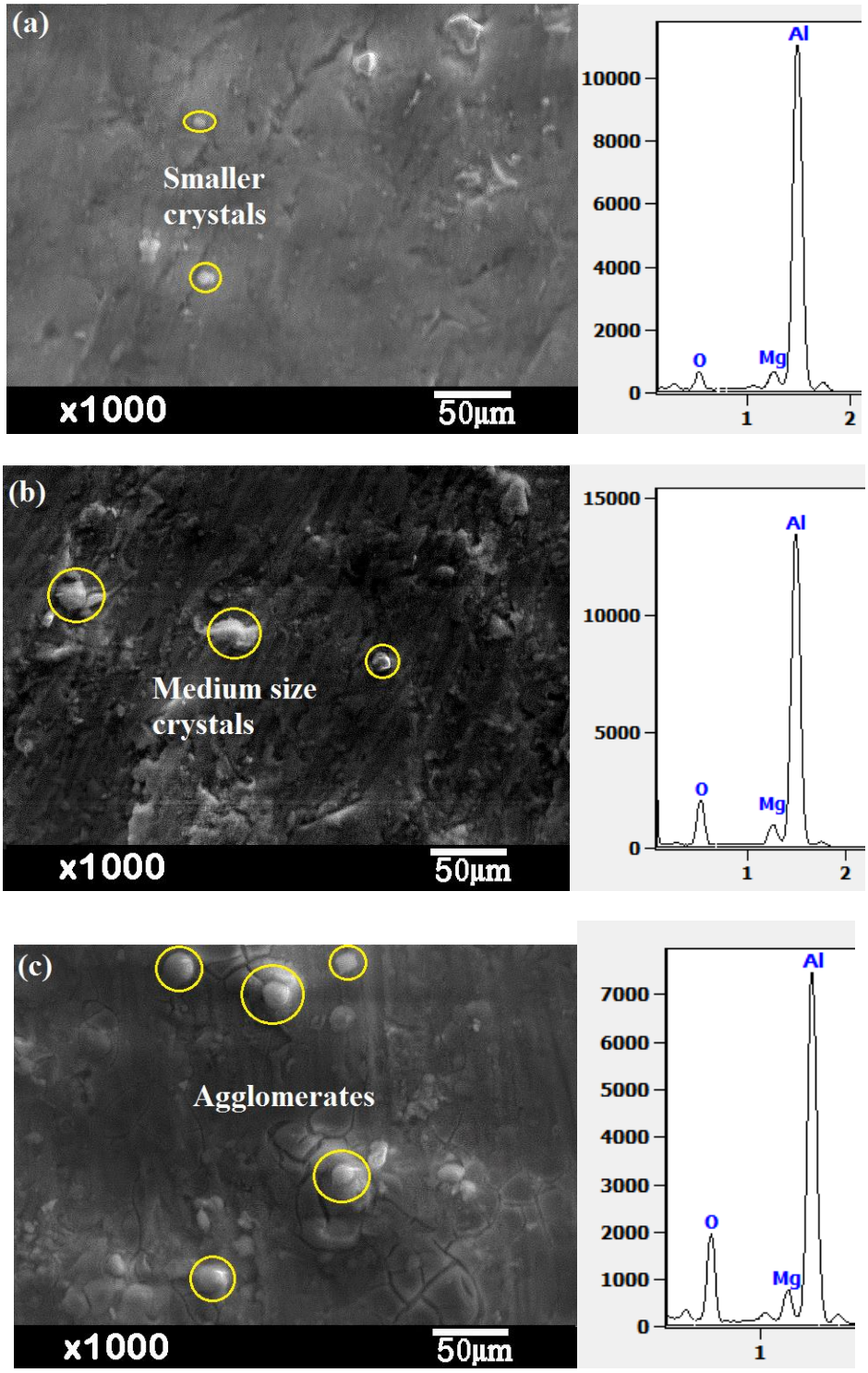

Figure 2.SEM micrograph and EDS spectra of the Al-4Mg/H_3BO_3 composite specimen (a) 1 wt % (b) 1.5 wt % and (c) 2 wt %.

Thus, it is confirmed that the $MgAl_2O_4$ formed in the composite is due to the addition of H_3BO_3 oxide source. The $MgAl_2O_4$ allows for heterogeneous nucleation in the molten melt and refines the structure (Figure 3a-c). $MgAl_2O_4$ has been reported as a stable oxide and potent nucleant of Al grains owing to its cube-on cube orientation relationship [27]. These potent nucleants tend to decrease the activation barrier for nucleation. As per the classical nucleation theory, this activation barrier greatly depends on

the interfacial energy between the nucleus metal and the nucleant for the heterogeneous nucleation. The decreasing level of activation barrier required for heterogeneous nucleation relies on the contact angle between the nucleus metal and the nucleant. The significant factor that affects the heterogeneous nucleation is the contact angle and it must be low as possible (lesser than 30°) for the nucleant to be highly potent. The lattice misfit between nucleating phase and nucleant must be low to reduce the interfacial energy to attain a low contact angle. The $MgAl_2O_4$ particles formed in the matrix has a low lattice mismatch and possess a similar cubic structure as that of aluminium hence it is a potent nucleant for the aluminium. A low misfit of 1.41 % between $MgAl_2O_4$ and aluminium is reported by Li et al. [27] on the (111) plane along the direction of [110]. $MgAl_2O_4$ possess a low lattice misfit to act as a potent heterogeneous nucleant. Nevertheless, its potency level relies on various parameters such as number density, particle size and narrow size distribution. A high amount and smaller size $MgAl_2O_4$ particles will result in better heterogeneous nucleation.

3.2. Corrosion behaviour

This study is performed to determine the corrosion performance of the composite specimens in three different solutions. 3.5 % NaCl solution is preferred since the sodium and chloride ions are present at greater levels in the marine atmosphere (seawater). Acidic and alkaline media are generally selected for study and hence the standard solutions of H_2SO_4 and HCl are used. Corrosion rate obtained for the Al-4Mg-H_3BO_3 (1, 1.5 and 2 wt %) composite specimens tested in three different solutions i.e., 3.5 % NaCl, 1 M H_2SO_4 and 1 M HCl at room temperature are displayed in Table 1.

Table 1. Corrosion test results of Al-4Mg/ H_3BO_3 composite

SOLUTION	**Parameters**	**1 wt% H_3BO_3**	**1.5 wt% H_3BO_3**	**2 wt% H_3BO_3**
3.5 % NaCl	E_{corr} (V)	-0.97	-0.93	-0.97
	i_{corr}(A/cm^2)	1.35E^{-05}	8.89E^{-07}	1.03E^{-05}
	Corrosion rate(mm/yr)	0.44	0.02	0.33
1 M H_2SO_4	E_{corr} (V)	-0.63	-0.64	-0.61
	i_{corr}(A/cm^2)	0.00011	3.82E^{-05}	9.09E^{-05}
	Corrosion rate(mm/yr)	3.79	1.248	2.96
1 M HCl	E_{corr} (V)	-0.71	-0.75	-0.76
	i_{corr}(A/cm^2)	0.0002	0.0001	0.0001
	Corrosion rate(mm/yr)	7.27	3.67	3.30

3.2.1. In the case of the 3.5 % NaCl solution, the corrosion rate of the Al-4Mg/1.5 wt% H_3BO_3 composite (0.029043 mm/yr) specimen is found lower than that of the Al-4Mg/1 wt % H_3BO_3 (0.44169 mm/yr) and Al-4Mg/2 wt % H_3BO_3 composite specimen (0.33594 mm/yr). The lower corrosion rate is due to lower corrosion current density of 8.89E^{-07} compared to other two composite specimens. The corrosion rate is higher for the low reinforcement fraction (1 wt % H_3BO_3) as there is no appreciable formation of $MgAl_2O_4$ and hence no grain refinement as observed in Figure 3a. The low corrosion rate obtained at 1.5 wt % H_3BO_3 is attributed to the grain refinement due to sufficient amount and reinforcement of $MgAl_2O_4$ without agglomeration. Increasing the H_3BO_3 causes agglomeration which might be increasing the corrosion rate.

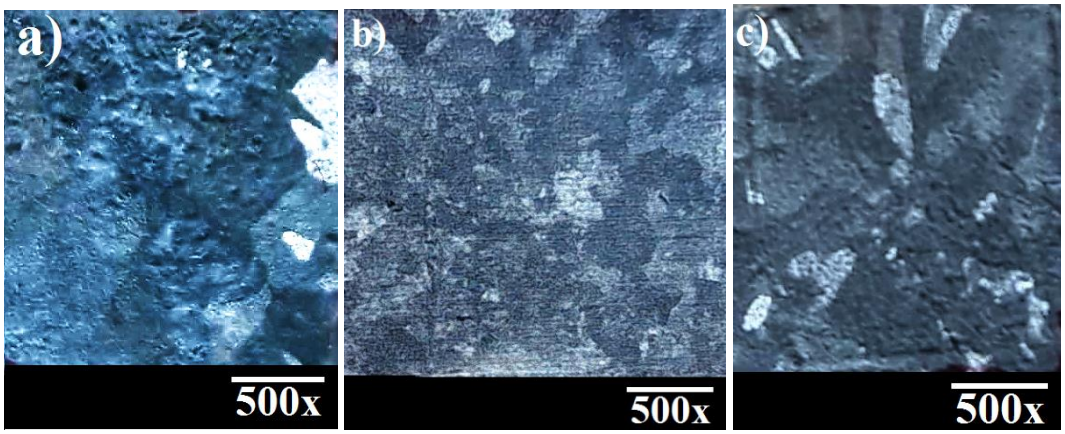

Figure 3. Grain refinement of Al-4Mg/H_3BO_3 composite a) 1 wt % H_3BO_3 b) 1.5 wt % H_3BO_3 and c) 2 wt % H_3BO_3

The SEM analysis results of the surface of the corroded specimen tested in 3.5 % NaCl is shown in Figures 4a-c. The pit density is quantified with the aid of Image analysis software Image J. The corroded surface of the specimens showed pits with the pit density increasing (15 %, 29 % and 35 %) as the H_3BO_3 level (1 wt %, 2 wt % and 3 wt %) increased respectively.

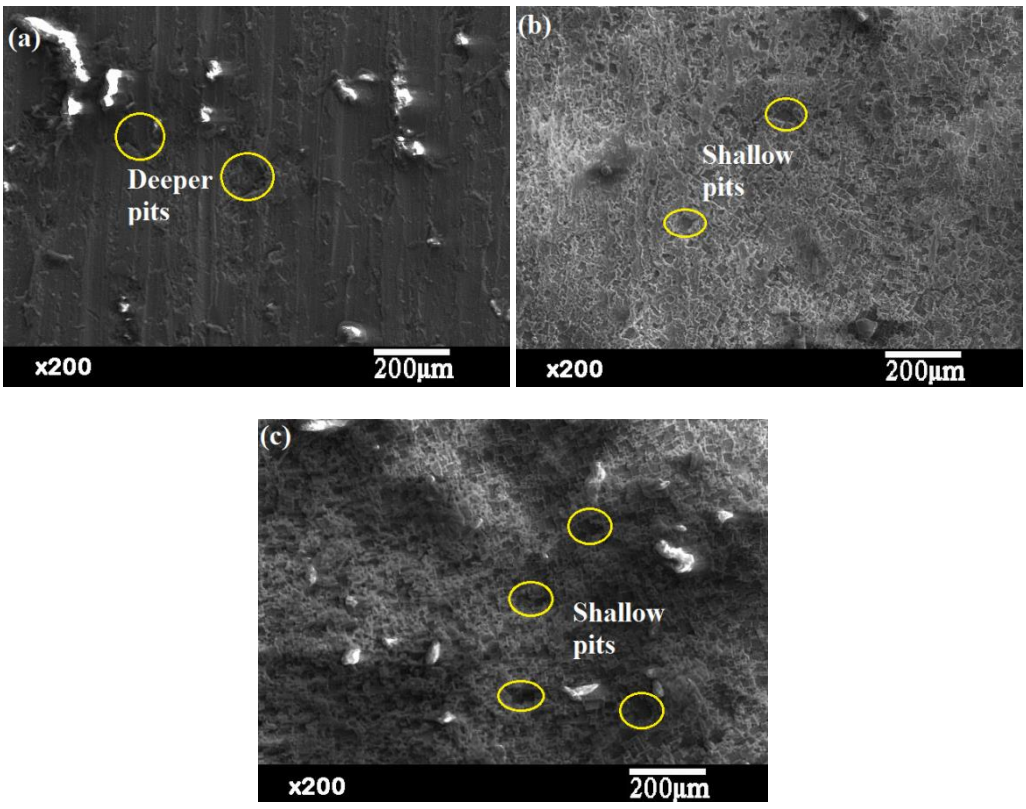

Figure 4. Corroded specimens tested in 3.5 % NaCl solution (a) 1 wt % (b) 1.5 wt % and (c) 2 wt%.

3.2.2. Similarly to 3.5 % NaCl solution, in 1 M H_2SO_4 the Al-4Mg/1.5 wt% H_3BO_3 composite specimen exhibited lower corrosion rate (1.248 mm/yr) than that of Al-4Mg/1 wt % H_3BO_3 (3.7973 mm/yr) and Al-4Mg/2 wt % H_3BO_3 composite specimens (2.9693 mm/yr). This is due to the lowest corrosion current density of $3.82E^{-05}$ obtained for the Al-4Mg/1.5 wt% H_3BO_3 composite specimen

compared to other two specimens. The corrosion trend is decreases initially upto 1.5 wt % and further increases when reaching 2 wt%. This is also attributed to the appreciable grain refinement produced by the $MgAl_2O_4$ crystals at the fraction of 1.5 wt% H_3BO_3. The SEM analysis on the surface of the corroded specimen tested in 1 M H_2SO_4 is shown in Figure 5a-c which is also agreeing with the trend of corrosion rate obtained for different fraction. The amount of corrosion products is determined through the Image analysis software Image J. The surface with 1 wt % H_3BO_3 (Figure 5a) revealed high amount of corrosion products (38 %) whereas 1.5 wt % reinforced composite surface (Figure 5b) showed mild pitting with lesser corrosion product (1.3 %).

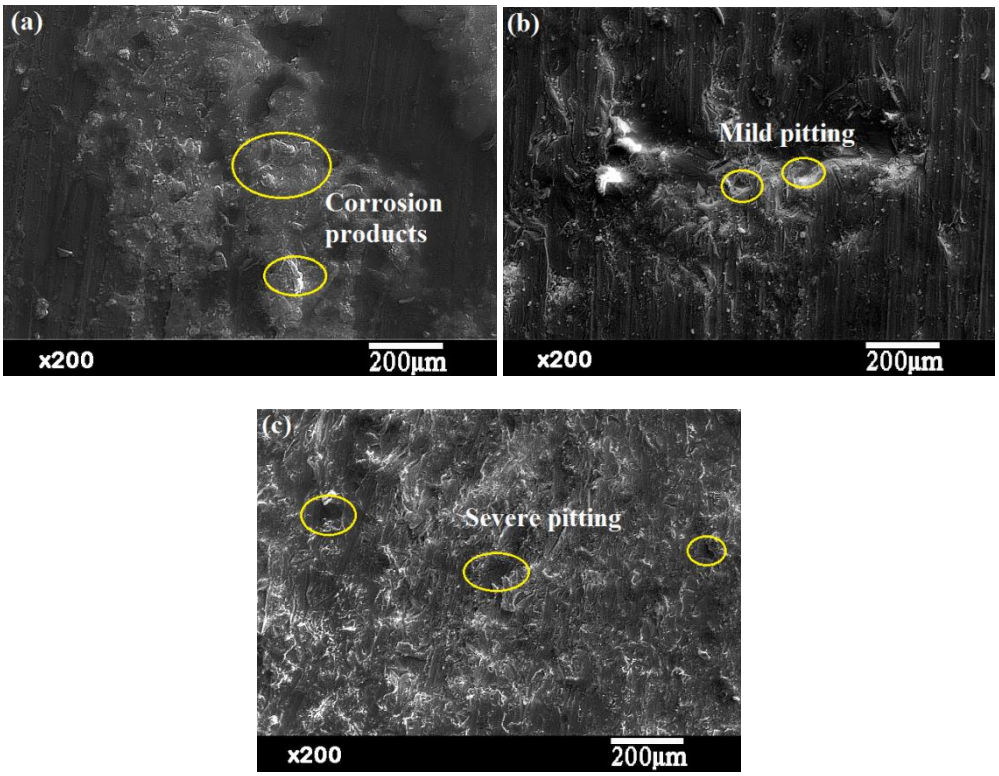

Figure 5. Corroded specimens tested in 1 M H_2SO_4solution (a) 1 wt % (b) 1.5 wt % and (c) 2 wt%.

3.2.3. In 1M HCl solution, the corrosion rate is found lowest in the case of the Al-4Mg/2 wt% H_3BO_3 composite specimen (3.3045 mm/yr) than that of the Al-4Mg/1 wt % H_3BO_3 (7.2793 mm/yr) and Al-4Mg/1.5 wt % H_3BO_3 composite specimens (3.6761 mm/yr). The corrosion rate is found initially higher at 1 wt H_3BO_3 and decreases as the reinforcement fraction increases. There is no appreciable difference in the corrosion rate of 1.5 wt % and 2 wt % H_3BO_3. In HCl, both the composites (1.5 wt % H_3BO_3 and 2 wt % H_3BO_3) possess better corrosion resistance. The SEM analysis on the surface of the corroded specimen tested in 1 M HCl is shown in Figure 6a-c. The corroded surface of the 1 wt % H_3BO_3 specimen (Figure 6a) revealed severe granular corrosion showing cracks on the surface evident the high corrosion rate (7.2793 mm/yr). The corroded surface of 1.5 wt % H_3BO_3 (Figure 6b) and 2 wt % H_3BO_3 (Figure 6c) composites indicates the moderate granular corrosion attack.

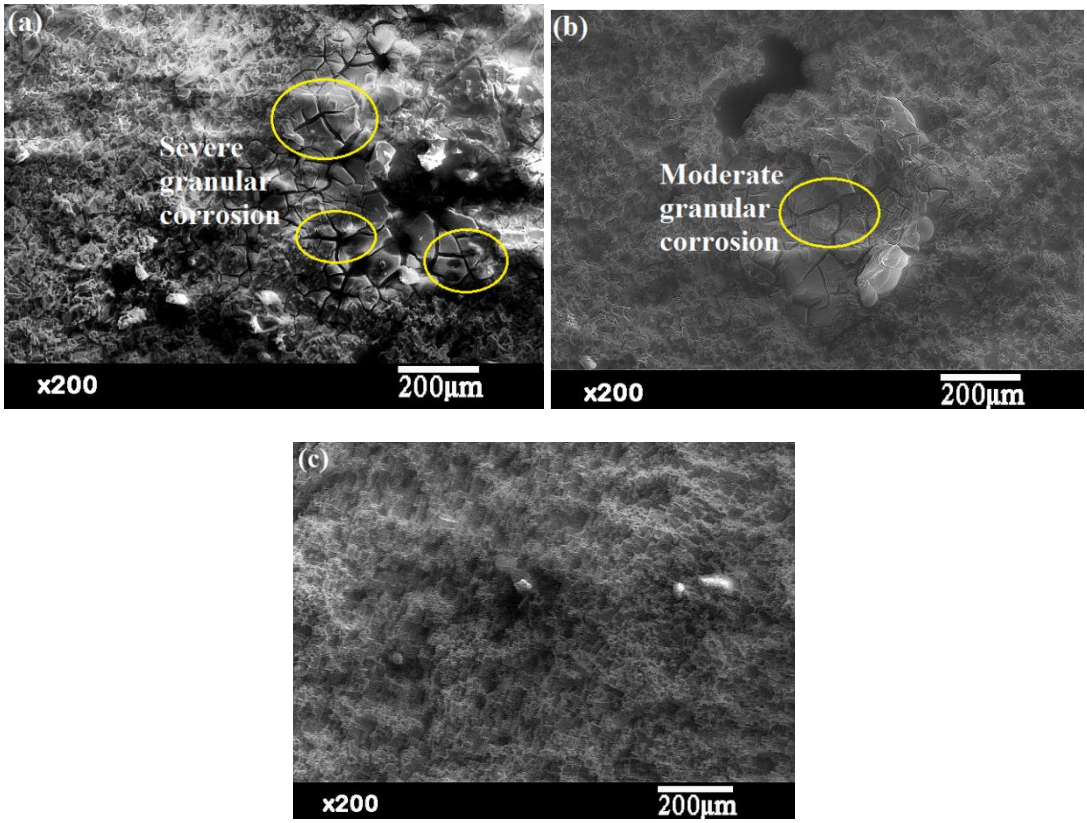

Figure 6. Corroded specimens tested in 1M HCl solution (a) 1 wt % (b) 1.5 wt % and (c) 2 wt%.

In 3.5 % NaCl and 1 M H_2SO_4, Al-4Mg/1.5 wt% H_3BO_3 composite specimen performed well relatively compared to the other two composite specimens (Table 1). Hence, Al-4Mg/1.5 wt% H_3BO_3 composite specimen can be utilized for the development of marine and naval applications exposed to NaCl environment. In 1M HCl, Al-4Mg/2 wt% H_3BO_3 composite specimen has better corrosion resistance in 1 M HCl compared to other two composite specimens (Table 1).

4. Conclusion

- In-situ Al-4Mg/$MgAl_2O_4$ composite specimens were fabricated successfully through the addition of H_3BO_3 (1 wt %, 1.5 wt%, 2 wt %) precursor.
- $MgAl_2O_4$ crystals were formed in all the composites upon addition of H_3BO_3 and slight agglomeration of $MgAl_2O_4$ crystals is observed in case of Al-4Mg/2 wt% H_3BO_3 composite.
- $MgAl_2O_4$ particles acted as heterogeneous nucleant in the Al matrix due to cube-on-cube orientation relationship and similar structure with aluminium.
- Corrosion rate is found to be lowest in case of Al-4Mg/1.5 wt % H_3BO_3 composite in 3.5 % NaCl and 1 M H_2SO_4 due to its lower corrosion current density and significant grain refinement by the $MgAl_2O_4$ particles.

Acknowledgement
The author gratefully acknowledge the technical and financial support from Indoshell Cast Private Limited, Coimbatore, India to carry out this research work.

5. References

[1] Mills J Robert, Lattimer Y Brian and Scott W 2018 *Corros. Sci.* **143** 1
[2] Holroyd N J H, Burnett T L, Seifi M and Lewandowski J J 2017 *Mater. Sci. Eng.* A **682** 613
[3] Yi G, Zeng W, Poplawsky J D, Cullen D A, Wang Z and Free M L 2017 *J. Mater. Sci. Technol.* 33 991
[4] Goswami R, Spanos G and Pao P S 2010 *Mater. Sci. Eng.* A **527** 1089
[5] Searles J L, Gouma P I and Buchheit R G 2001 *Metall. Mater. Trans.* A **32** 2859
[6] Scotto D, Antuono D, Gaies J and Golumbfskie W 2014 *Scr. Mater.* **76** 81
[7] Zhang R, Gupta R K, Davies C H J, Hodge A M, Tort M, Xia K and Birbilis N 2015 *Corros.* **72** 160
[8] Zhang R, Qiu Y and Qi Y 2018 *Corros. Sci.* **133** 1
[9] Li, Zhang Z and Vogt R 2011 *Acta. Mater*. **59** 7206
[10] Gupta R K, Zhang R, Davies C H J and Birbilis N 2014 *Corros*. **70** 402
[11] Wang Y, Gupta R K, Sukiman N L, Zhang R, Davies C H J and Birbilis N 2013 *Corros. Sci.***73** 181
[12] Carroll M C, Gouma P I, Mills M J, Daehn G S and Dunbar R 2000 *Scr. Mater.* **42** 335
[13] Zhang R, Gupta R K, Davies C H J, Hodge A M, Tort M, Xia K and Birbilis N 2015*Corros.***72** 160
[14] Liu S Q, Wang X, Cui C X, Zhao L C, Liu S J and Chen C 2015 *Mater. Des.* **65** 432
[15] Liu S Q, Wang X and Cui C X 2017 *J. Alloys Compd.* **701** 926
[16] Liu S Q, Cui C X and Wang X 2018 *Appl. Surf. Sci* .**431** 202
[17] Liu S Q, Cui C X and Wang X 2017 *Met.* **7**2 04
[18] Ali Torkan, Amin Rabiei Baboukani and Iman Khakpour 2018 *Nanosci. Nanometro.* **4** 34
[19] Liu S, Wang X and Tao Y 2019 2019 *Appl. Surf. Sci*. **484** 403
[20] Sadegh Rasouli, Reza A Behnagh, Abdolrahman Dadvand and Noureyeh Saleki-Haselghoubi 2014 *J Mater. Des.Appl.* 1
[21] Prabhakar G V N B, Ravi Kumar N and Ratna Sunil B 2018 *Mater. Today: Proceed.* **5** 8391
[22] Meijuan Li, Kaka Ma, Lin Jiang, Hanry Yang, Enrique J. Lavernia, Lianmeng Zhang and Julie Schoenung 2016 *Mater. Sci. Engg.* A **656** 241
[23] Ranjit Bauri, DevinderYadav, Shyam Kumar C N and Balaji B 2014 *Mater.Sci. Engg.* A **620** 67
[24] ChengGuo, TianchunZou, Chunsheng Shi, Xudongyang, Naiqin Zhao, Enzuo Liu and Chunnian He 2015 *Mater. Sci. Engg.* A **645** 1
[25] Zhenyang Yu, Naiqin Zhao, Enzuo Liu, Chunsheng Shi, Xiwen Du and Jian Wang 2012 *Compos. Part A* **43** 631
[26] Li Xing, Yaxuan Zhang, Chunsheng Shi, Yang Zhou, Naiqin Zhao, Enzuo Liu and Chunnian He 2014 *Mater. Sci. Engg.* A **617** 235
[27] Li H T, Wang Y and Fan Z 2012 *Acta. Mater.* **60** 1528